Design of laser-textured surfaces to enhance the strength of adhesively bonded joints

DESIGN OF LASER-TEXTURED SURFACES TO ENHANCE THE STRENGTH OF ADHESIVELY BONDED JOINTS

F. Moroni [a], L. Romoli [a], M.M.A. Khan [b,*]

a Department of Engineering and Architecture, University of Parma, Italy
b Department of Industrial and Production Engineering, Shahjalal University of Science and Technology, Bangladesh

Abstract

This paper tries to relate the laser treatment process parameters to the morphological properties of laser-treated aluminum alloy surfaces and the adhesive joint fracture load in butt joint configuration to describe their pivotal role as surface roughness design parameters. In these contexts, the role of the individual process parameter and energy density on the surface and joint characteristics were experimentally investigated. Surface roughness was modeled and validated to demonstrate that it is designable and controllable. Moreover, to globally understand the effect of the laser parameters on joint fracture load, experimental results were analyzed following a DoE framework. This study shows that laser-treatment parameters contribute significantly to surface roughness control. Model-based surface morphology and the consequent average surface roughness can be accurately predicted, i.e., groove characteristics of the surface can be accurately controlled by regulating the laser-treatment parameters. Optimal laser parameters allow designing a surface that maximizes the adhesive joint fracture load.

Keywords: Laser, Surface modification, Adhesive Bonding

1. Introduction

Adhesive bonding is a technique that promotes its application field for joining different materials since using adhesive reduces the cost and the weight of the structures. Unlike traditional joining techniques, e.g., riveting, bolting, etc., this technique requires no holes and hence may reduce stress concentration problems if compared to previous ones and offers no damage to the parts being joined. Besides, this type of bonding raises service life of the components and lowers corrosion development and machining cost [1].

In adhesive joining, the adhesion between adhesive and substrates takes place due to adhesive penetration in surface roughness, and hence, adhesion level relies partly on the adherend surface quality characterized by surface roughness. For adhesive joints, the roughness of adherend surfaces is, therefore, frequently used as a design parameter. In this context, several researchers have investigated its effect on adhesively bonded joint strength [2]. Ghumatkar et al. [3] performed an experimental investigation on the effect of adherend surface roughness on adhesive bond strength and found an optimal surface roughness for a maximum bonding shear strength. Similar results were also found for tensile strength [4] and fatigue life [5] for different joint configurations. Rudawska [6] performed a survey on the influence of surface roughness obtained by grinding, lapping and superfinishing treatment on the strength of bonded joints. The results displayed an inverse dependence between the surface roughness and joints strength for grounded and super finished joints. On the opposite, when the surfaces were lapped, the higher was their roughness; the higher was the joints strength. Da Silva et al. [7] studied the effect of macroscopic grooves (between 0.1 and 0.3 mm in depth) on the tensile strength of single lap joints. The grooves were produced by a milling machine equipped with a cutting bit. The experimental tests proved that the presence of grooves significantly increases the interfacial joints strength promoting a cohesive failure, especially for stiff adhesive. Kim et al. [8] investigated the effect the surface topography on adhesion strength. In particular, in the presence of micropatterns, they asserted that the joints strength is increased by the transition of the failure mode from interfacial to cohesive. There is, however, no published article, which attempts to regulate the groove characteristics of the surface roughness, i.e., depth and width of groove determining the surface roughness.

Again, the majority of the untreated surfaces comprises comparatively small in shape incompatible unevenness. Hence it is preferable for the adherend surfaces to undergo a suitable surface treatment to secure the desired level of interfacial strength. Surface treatment methods can be mechanical, chemical, electrochemical and laser surface texturing, etc. Though all these

treatments cause some degree of change in surface roughness, laser ablation treatment shows its promise in obtaining the desired level of surface roughness [9]. Zhang et al. [10] performed surface pre-treatment using an excimer laser and found that bonded joint strength improved significantly for the laser-treated samples as compared to mechanically abraded ones. Stammen et al. [11] showed that laser surface pre-treatment allowed yielding a surface that provides better bonding performance and aging-resistant aluminum joints. Rotella et al. [12] also noted that laser surface modification provided favorable changes in surface roughness resulting in enhanced adhesive joint strength. Together with changes in roughness, laser ablation treatment also provides surface cleansing [13] and modification of the surface chemical composition. In particular, as shown in [14], the pulsed laser treatment produces a thick aluminum oxide layer, which improves the wetting properties.

The laser surface-treatment process parameters govern the profile of the track left on the material. Since the repetition of multiple tracks generates an almost periodic surface, such surface features are commonly known as ‘grooves’ to encompass also narrower and deeper valleys [14]. This term will be adopted throughout the manuscript to describe the features characterizing the surface roughness. Thus, the process parameters influencing the grove profile need to be optimized to obtain optimal surface roughness and joint strength.

Conventionally, engineers or machine operators use their skills to choose the laser surface-treatment process parameters to obtain the surface roughness, which provides the joint with the required strength and then the joint is tested to make sure that the joint is meeting the designed specification. Eventually, the process input parameters thus selected yields a joint close to the required specification. Therefore, this not only comes out to be a time consuming and error development effort but also fails to achieve the optimized laser surface texturing parameters. Response Surface Methodology (RSM), on the other hand, can predict the process input parameters accurately without consuming time, materials and labor efforts and be used to achieve a reasonable relationship between process input parameters and the desired responses [15]. These, in fact, motivate many researchers to apply an RSM for predicting and optimizing bonded composite-steel single lap joining [16] and friction stir welding of aluminum alloy [17]. However, to date, optimization of the laser surface roughness-mediated joining process parameter using RSM to maximize the adhesive joint fracture load, a measure of joint strength, is lacking.

1.1 Research objectives

The main objective of this study is to design the roughness of a surface to enhance the fracture load of adhesively bonded joint in butt joint configuration. This study, therefore, focuses on:

- Investigating the effects of laser surface roughness-mediated joining process parameters on surface roughness characteristics to understand their roles in controlling the surface roughness and hence, the adhesively bonded joint fracture load;
- Modeling the surface roughness characterized by surface groove features to illustrate the fact that surface roughness can be accurately designed and controlled;
- Using the response surface methodology to avoid the obvious difficulties in correlating the areal roughness with the joint fracture load. For this purpose, the final goal will be to obtain an optimal set of laser surface roughness-mediated joining process parameters that would allow designing the roughness of a surface providing the maximum fracture load of the joint.

2. Experimental set-up

2.1 Specimen preparation

Aluminum alloy substrates (AA6082 – T4) were bonded together with a two-component epoxy adhesive (Loctite Hysol 9466) to make a tubular butt joint. The joint under investigation was a hollow circular section with a wall thickness of 5 mm, showing an as-received roughness of about 1 µm. This typical bonded joint was considered from both the technical and economic viewpoints as it can provide an acceptable service performance and substantial savings. After machining the substrates to the designed size and shape, they were subjected to a basic cleaning process (soap and water) to remove dust and oil. Once the substrates

became completely dry, the surfaces were treated with an Nd:YVO_4 laser to alter the surface roughness. Finally, to prepare the specimen, the substrates were then assembled applying the stated adhesive which was cured in an oven for 1h at 80°C.

2.2 Laser surface treatment

The surface modification of aluminum alloy adherends was performed using an Nd:YVO_4 fiber laser (LaserPoint YFL 20P), with a wavelength of 1064 nm, working in pulsed operating mode. The focus adjustment was ensured by a high precision z-axis positioning system, while the laser beam was moved on the surface using a Galvo-mirror scanner. The equipment can generate a maximum average laser power of 20 W and, since a repetition rate (RR) of 20 kHz was selected, the energy associated with each pulse is approximately 0.1 mJ. The pulse length is shorter than 120 ns (Pulse Width Half Maximum). For the present work, a 20 kHz Repetition Rate was preferred since it provided for the highest pulse energy and a consequent more vigorous material ablation. Such an effect increased the number of microscale asperities which were found to contribute significantly to the interlocking phenomena at the interface between the adherend and the adhesive. The laser beam is collimated and then focused on the surface: the resulting spot size ($Ø_{spot}$) is evaluated to be approximately 35 µm. To cover the entire specimen hollow circular section, the laser beam was moved along concentric paths; therefore, the first treatment parameter is represented by the distance between two adjacent paths (hatch distance, H). The other two treatment parameters evaluated in this work are the tangential scanning speed (V) and the average laser power (P). The range of variation of each parameter is shown in Table 2.1.

Table 2.1: Variation in individual process parameter

Treatment Parameters		Minimum Value	Maximum Value
Hatch Distance	H [mm]	0.033	0.117
Scanning Speed	V [mm/s]	62	1238
Average Power	P [W]	10	20
Repetition Rate	RR [kHz]	20	Fixed
Spot size	$Ø_{spot}$ [µm]	35	Fixed

Though the material ablation process is pulsed, the action of a moving beam can be approached using the concept of Energy Density, ED expressed in J/mm^2 and defined as [18]:

$$ED = \frac{P}{V \cdot Ø_{spot}} \quad (1)$$

The variation of P and V reported above, and the constant $ø_{spot}$ resulted in ED in the range of 0.230-9.216 J/mm^2.

2.3 Surface characterization

A Taylor Hobson 3D optical profiler was used to characterize the ablated surfaces. An example of laser ablated surface is given in fig. 2.1 to show the periodicity of the surface generated by the partial superposition of the grooves. The distance between the deepest points of each groove represents the hatch distance H. A contactless measuring technique was preferred to a stylus rough meter which showed severe limitations in reaching the bottom of extreme aspect ratio grooves generated at the highest values of the energy density. The resolution of the instrument on the XY-plane was 340 nm. This value is related to the diffraction limits of the light of the green diode used. While the resolution on the Z-axis was nearly 1 nm. The morphology maps (square area, 400 µm x 400 µm) acquired were used to derive the average areal roughness Sa according to ISO 25178-2. Areal roughness was used to characterize the surface because of its most extensive use in mechanics even though a broader characterization should involve other relevant amplitude parameters (e.g., Surface Skewness, Kurtosis, Density of peaks, etc.).

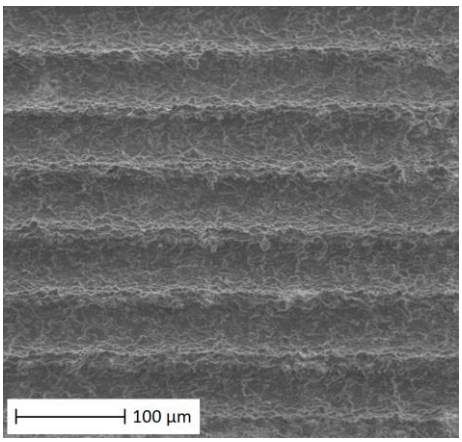

Fig. 2.1: Example of a laser treated surface morphology

2.4 Experimental design

Because the adhesion between adhesive and substrates as well as the cohesion of the adhesive layer after curing determines the adhesive bond strength, it is necessary for the adherend surfaces to undergo a suitable surface treatment to achieve an acceptable bonded joint quality. In this study, Nd:YOV_4 based laser system was used to modify the surface roughness of the substrates. Three factors five levels central composite rotatable experimental design with full replication was applied to plan the experiment. The laser surface texturing input variables considered were average laser power (P), scanning speed (V), and hatch distance (H). Design-Expert V7, the statistical software, was used to construct the design matrix consisting of a set of treatment combinations using response surface methodology (RSM); to develop a statistical model by fitting joint fracture load data obtained from the experiments to various equations taking linear, two-factor interaction, quadratic and cubic terms of the process input variables (i.e. laser power, scanning speed, and hatch distance) into consideration sequentially and finalize the statistical model for joint fracture load by using various statistical estimates and eliminating the input variable(s) that have statistically insignificant impact on the joint fracture load so as to improve the model's performance in predicting the variation in joint fracture load within the design space; and finally to determine the optimal set of process parameters using its numerical optimization function. Each combination was replicated three times to ensure the repeatability of the experiment and estimate the variability associated with the experiments needed to validate the statistical model developed for the joint fracture load.

On the way to find the range of each process input parameter, initial trial runs were carried out by changing one of the process parameters while keeping others at constant values. Table 2.2 shows primary input factors, their corresponding coded and actual levels, and response factors considered.

Table 2.2: Experimental conditions and response factors

PROCESS FACTORS	SYMBOLS	LIMITS				
		-2	-1	0	+1	+2
Avg. laser power (W)	P	10	12	15	18	20
Scanning speed (mm/s)	V	62	300	650	1000	1238
Hatch Distance (mm)	H	0.033	0.05	0.075	0.100	0.117

CONSTANT FACTORS		
Adherend material	:	Aluminum alloy (AA6082-T4)
Adhesive	:	Epoxy adhesive (Loctite Hysol 9466)
Laser source	:	PW Nd:YVO_4 laser

Response Factors		
Surface characteristic	:	Surface roughness (S_a)
Joint Characteristic	:	Joint fracture load (JF)

Response surface methodology (RSM) was applied using the same software to optimize the laser surface roughness-mediated adhesive joining process parameters numerically. At this stage, the core target was to determine the optimal set of process parameters ensuring the optimal adhesively bonded joint fracture load. The quality criteria defined for the bonded joint to determine the optimal settings of joining process parameters were the maximization of the fracture load of the bonded joint keeping the surface roughness in the range.

2.6 Mechanical characterization

After joining, an Instron 4400 electromechanical testing machine equipped with a 30 kN load cell was used to determine the fracture load of the bonded joint. In this study, each test was designed and conducted taking ASTM D897-08 [19] as a reference. The specimen proposed in [20] and schematically shown in Fig. 2.1 was used to obtain a reliable result. The joint was designed to obtain an almost uniaxial tensile stress field, to ensure good control of the adhesive thickness and the substrate coaxially, without the requirement of additional jigs, to facilitate the joints manufacturing. The reference surfaces located in the middle of the specimen were used to control the axial alignment of the two substrates and the adhesive layer thickness (set to 0.3 mm). The bonded area was closed with a Teflon (PTFE) spacer placed between the two substrates. The latter, therefore, results in a hollow circular section with the dimensions shown in Fig. 2.1. The through hole was made to clamp the specimen during the adhesive polymerization, and the threaded hole was utilized for applying the load. The sample was linked to the testing machine using spherical joints.

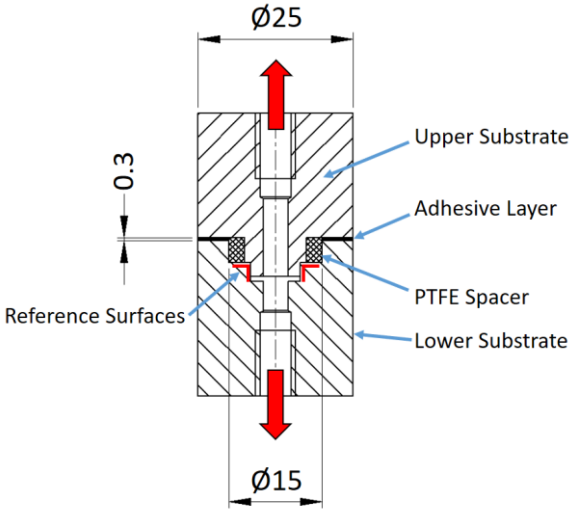

Fig. 2.1: Specimen geometry (dimension in mm)

3. Results and discussion

3.1. Parametric effect on surface roughness characteristics

In this study, surface roughness has been considered as a measure of surface characteristics. Fig. 3.1 is a perturbation plot illustrating the effect of individual laser surface roughness-mediated joining process parameter on surface roughness. The graph represents a first elaboration of the results, aiming to provide a graphical representation of the effect of the process factors in table 2.2 at the point located in the middle of the design space (P = 15W, V = 650 mm/s, H = 0.075 mm). It is a graphical indicator of the factors' effect: the steeper is the slope, the higher is the effect of the factor over the response. Curvature pattern of the line means the response factor changes nonlinearly with the input variables.

From fig 3.1, it is clear that surface roughness increases and decreases significantly with the average laser power and scanning speed respectively. This is because increased laser power helps energy density input to interact more with the surface material under focus and consequently, the surface becomes rougher. On the other hand, higher scanning speed lessens the interaction time and hence, reduces the interaction of energy input with the surface material. As a result, surface roughness decreases as a consequence of increased scan speed. Besides, the hatch distance is found to have a slight influence on the surface roughness although an inverse-U relationship can be appreciated from fig. 3.1. This phenomenon can be explained considering that when grooves are partially superimposed the surface roughness increases with increasing their spacing (Hatch Distance parameter) up to the limiting value for which the superposition is no longer present (hatch distance approximately equal to the laser spot diameter). Conversely, when groove profiles are separated from one another, an increase in hatch distance results in a lower roughness.

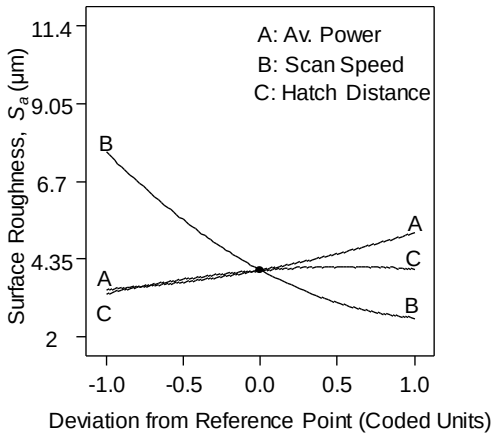

Fig. 3.1: Perturbation plot showing the effect of laser parameters on surface roughness, S_a *(*AA*: Avg. Laser Power,* BB*: Scanning Speed,* CC*: Hatch Distance).*

Fig. 3.1 also shows that surface roughness varies nonlinearly with each of the laser surface roughness-mediated joining process parameters. However, these are not the only variables affecting the surface roughness. It has been reported that energy density, a function of two laser parameters under consideration (i.e., a combination of laser power and scanning speed for a constant laser spot diameter), may contribute to the change of surface roughness and the bonded joint strength [20]. Therefore, the role of energy density in controlling the surface roughness and the joint fracture load was investigated.

3.2 Role of energy density in surface roughness and joint fracture load control

Fig. 3.2 illustrates how the energy density, a laser surface roughness-mediated joining process parameter in energy term, plays its pivotal role in controlling surface roughness (S_a) and joint fracture load (JF) for a specific constant hatch distance (H = 0.075 mm). From this figure, it is evident that both the surface roughness and the joint fracture load are energy-limited. With an increase in energy density, surface roughness rises almost linearly up to the limiting value of about 4 J/mm² and then gradually decreases. This is because higher energy density input results in localized melting and flattening of the crest with a consequent reduction in roughness of the surface. Taking into account that the adhesive joint fracture load was measured to be 12 kN for untreated adherends with S_a nearly 1 µm, results showed that when ED used is closer to the typical material threshold; only slight effects are generated on the surface. This is represented by the point at ED = 0.215 J/mm^2, for which S_a of about 2 µm is achieved, resulting in no enhancement of JF with respect to the untreated surface (not represented in fig. 3.2). Conversely, when the specific energy density threshold is overcome, relevant effects are induced on JF: for ED = 0.438 J/mm^2 generating S_a = 3.2 µm, JF reaches nearly 16 kN which represents an increase of 30% with respect to the untreated surface. The sudden jump in the joint fracture load between the untreated surface and the areal roughness of 3.2 µm is related to the nature of the onset of laser ablation which is indeed a step-like process.

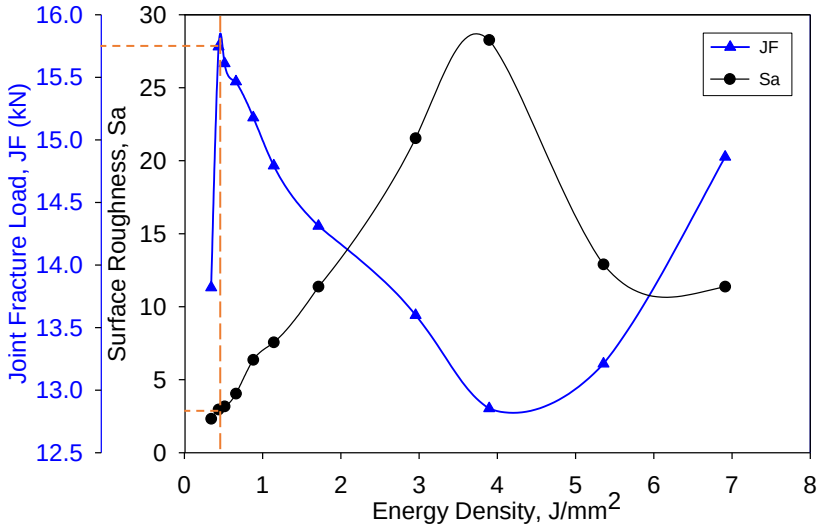

*Fig. 3.2: Variation in joint fracture load (*kN*) and surface roughness (*µm*) with energy density for a constant hatch distance* H = *0.075 mm*

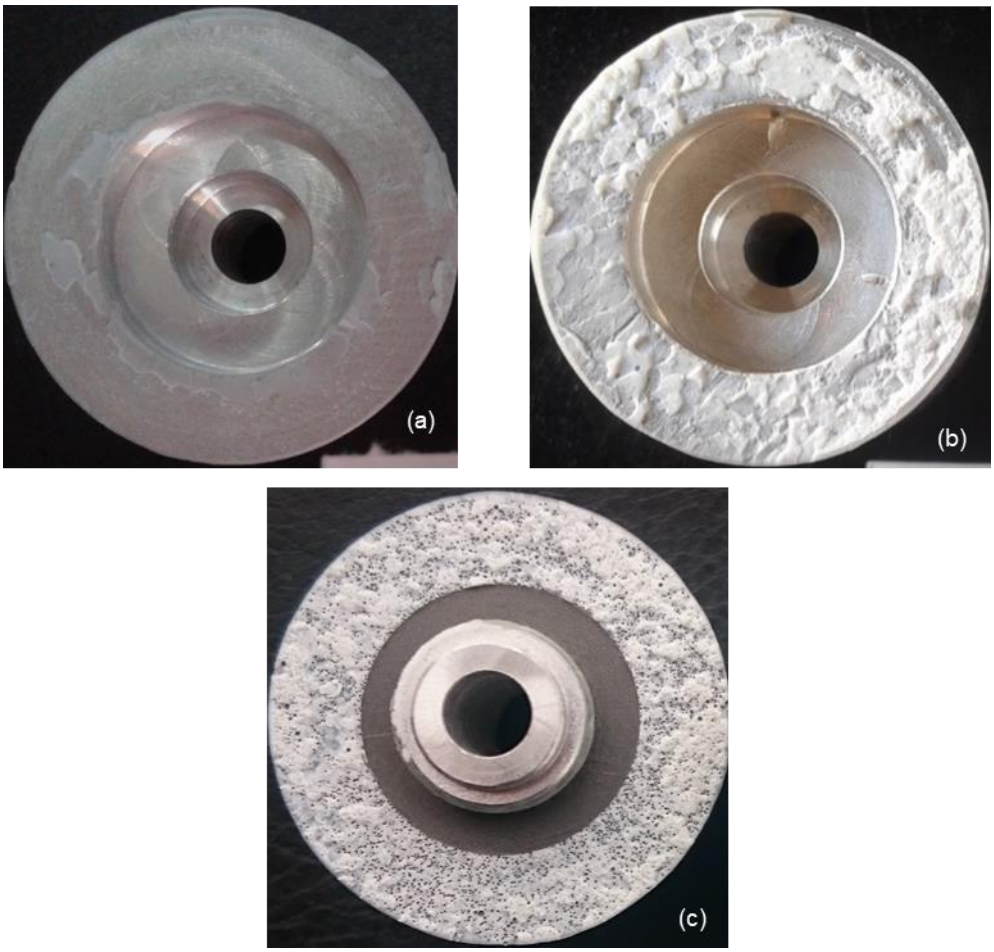

Figure 3.3: Surface fractures of joints treated with different ED *values (a:* ED = *0.33 J/mm² - b:* ED = *0.66 J/mm² - c:* ED = *3.89 J/mm²)*

Also, this figure demonstrates that the surface roughness limits the adhesive joint fracture load, i.e., bonding fracture load rises steeply with an increase in adherend surface roughness up to a certain point, i.e., S_a = 3.2 µm and then starts to decrease

gradually beyond this limiting value. This trend indicates the fact that continuous increase in surface roughness does not provide any assurance for continuous improvement in fracture load of the adhesive bonded joint. These phenomena can be understood by observing the fractured surfaces and can be traced back to the following facts: when a low energy treatment is performed, the surface is not significantly modified, and the joint surface fractures show a predominantly adhesive failure (Fig 3.3 - a). An increase in ED makes the treatment able to modify the surface morphology producing a rougher surface. The induced wedging effect increases with the increased roughness of the adherend surface and this makes the attachment of the adhesive stronger, leading to a utterly cohesive failure (Fig 3.3 - b); beyond the limiting point, any increase in surface roughness raises the possibility of entrapment of the air bubbles within the grooves of the adherend surfaces weakening the bonding fracture load of the joint. This is confirmed by the fracture surface shown in Fig 3.3 – c, where an utterly cohesive fracture can be noticed (the interface strength between adherent and adhesive is good), although a significant amount air bubbles can be identified.

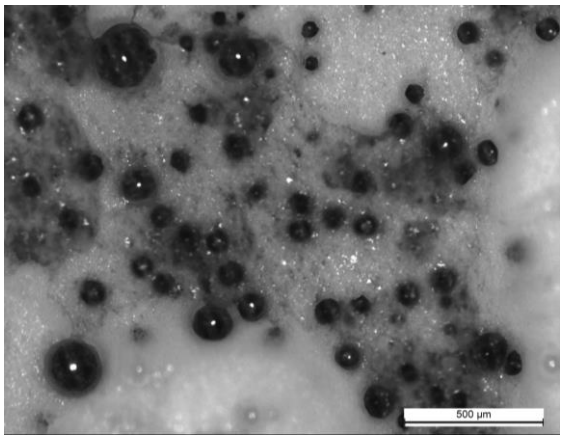

Figure 3.4: Optical microscope observation of fractured surfaces of the specimens shown in Fig 3.3 – c.

Fig. 3.4 shows an example of a fractured surface, observed by means of an optical microscope. The picture refers to the specimen shown in Figure 3.3 (c). The bubbles are predominately located close to the interface between adhesive and substrate and they lead to a reduction of the bearing area in the range between 15 and 20%. The bubbles size is in the range between 15 and 80 µm.

The laser parameters affect the groove characteristics of the surface, which in turn determine the surface roughness and again, in turn, the air entrapment phenomenon and the joint fracture load. Therefore, the surface roughness was modeled to illustrate the fact that surface roughness can be designed, modified and regulated by the proper selection of the aforementioned parameters.

3.3 Modelling of surface roughness

In order to predict the surface roughness (S_a) of laser treated surfaces, the influences of P and V (and as a consequence of energy density) on a single groove were initially studied. The model is designed to be applied to any kind of material assumed that the energy delivered by the laser is absorbed with a nearly negligible thermal conduction. This is true within the limits of an ablation process ruled by fast scan speed and pulse duration shorter than 100 ns. Dimensions of singles laser ablated grooves were obtained for different parameters combinations by extracting profiles as reported in Fig. 3.5. According to the observation of the surfaces similar to that reported in Fig. 2.1, flanking adjacent grooves with a partial superposition defined by the parameter H ablate the bulges along the edges of single grooves. Within the limits of an ablative process which does not thermally affect the workpiece (meaning that liquid phase is negligible), the surface pattern results composed by an almost periodic series of grooves with no protrusions at the edges. In order to model such pattern for each groove profile, a theoretical plane was defined considering the external portions of profile that were not involved in the laser ablation. The aim is to filter from the groove profile eventual deposits of debris and ejected material at the groove edges, as well as any other form of a protrusion. The definition of the groove depth concerning the theoretical mean plane is done in accordance with ISO 25178-2 for the further definition of S_a.

Taking into account the nearly Gaussian profile of the beam and the Beer-Lambert absorption law, the groove profile was evaluated with a parabolic function fitting the acquired data. The maximum groove depth, D was calculated as the distance between a minimum of the parabolic function and the theoretical plane while the groove width, W was calculated as the distance between the intersections of the parabolic function with the plane mentioned above, as shown in Fig. 3.5.

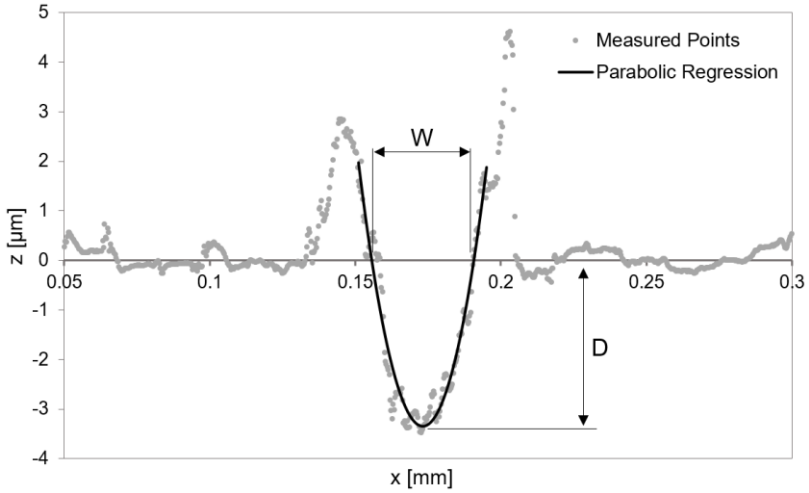

*Fig. 3.5: Definition of Width (*W*) and Depth (*D*) from the acquired profile.*

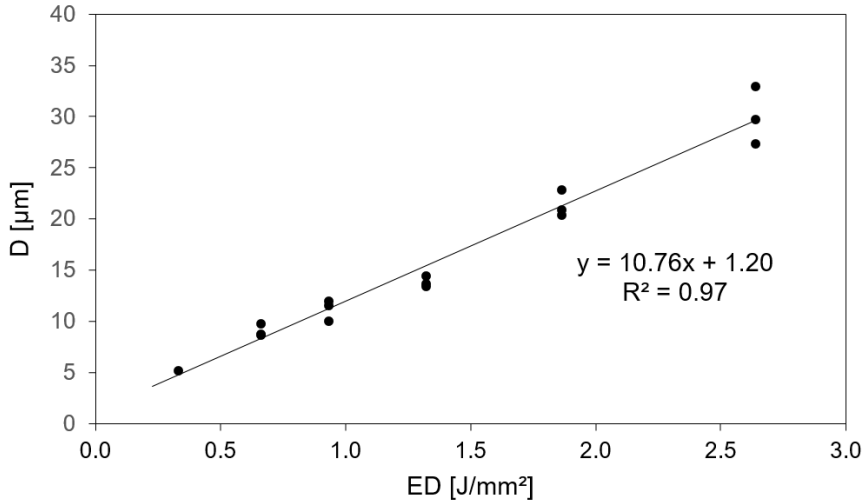

*Fig. 3.6: Groove Depth (*D*) as a function of* ED*.*

The average groove depth, D calculated over four measurements (two different positions for the two separate grooves) is reported in Fig. 3.6 as a function of energy density. Depth was found to increase linearly with energy density in the tested range, and a regression was used to derive the analytical expression correlating groove depth, D.

Conversely, the average width, W cannot be unambiguously described as a function of energy density. Values reported in Fig. 3.7 show a slightly different behavior for the three levels of average power used: for 20 W the width slowly increases with energy density while it remains almost constant to 55 µm for 15 W and it decreases for 10 W. The latter trend could be explained considering that, for lesser power, thermal losses are also lower with a consequent reduction in energy conduction on a plane perpendicular to the optical axis. Therefore, despite the values registered oscillated around the double of the focused beam diameter, for the sake of clarity, three different behaviors of groove width, W with energy density have to be considered.

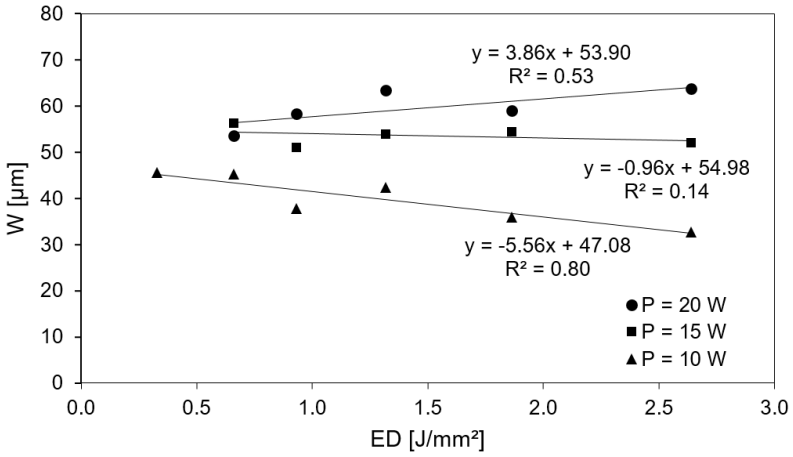

*Fig. 3.7: Groove Width (*W*) as a function of* P *and* ED*.*

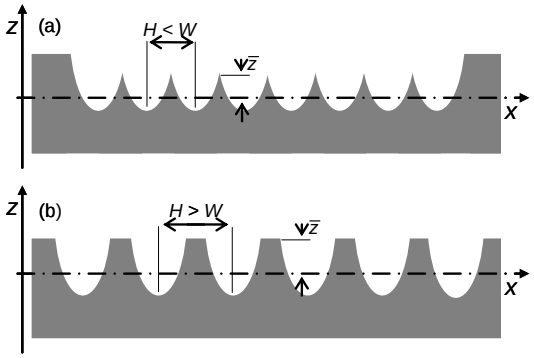

Fig. 3.8. Scaled sketch for the theoretical calculation of S_a *as a function of* H*: (a)* H < W *and (b)* H > W *for a constant* ED*.*

If the surface pattern is deemed to be formed by grooves placed side by side, then a cross-section perpendicular to the grooves direction is representative for the alternation of peaks and valley characterizing the roughness. The influence of hatch distance, H on surface roughness, S_a consists merely of the two possibilities represented in Fig. 3.8. Surface roughness, S_a should decrease by reducing H as in panel (a) where hatch distance, H is narrower than groove width W, and the grooves are partially superimposed. In panel (b) hatch distance, H is larger than groove width, and surface roughness has an opposite dependence on hatch distance relating to the previous case. The first step accounts for the definition of the mean line: this is done by balancing the areas of valleys and those of the crests. The model takes into consideration the parabolic profile of the laser ablated groove, and the areas underneath the profile determined by the intersection of adjacent profiles were analytically calculated by integrating the parabolic function within the geometrical boundaries. The reference z position of the mean line turns out to be:

$$H < W \qquad \bar{z} = \frac{2}{3}\left(\frac{DH^2}{W^2}\right) \qquad (2)$$

$$H \geq W \qquad \bar{z} = \frac{2DW}{3H} \qquad (3)$$

Taking into account the definition of S_a as the average value providing the same area of the defined peaks and valleys over the hatch distance H (according to ISO 25178-2), S_a can be calculated for H < W and H ≥ W in Eq. 4 and Eq. 5, respectively. The surface roughness increases with squared H up to H = W and then it inverts its dependence on H.

$$H < W \qquad S_a = \frac{4}{9\sqrt{3}}\left(\frac{DH^2}{W^2}\right) \qquad (4)$$

$$H \geq W \qquad S_a = \left(\frac{4DW}{3H}\right)\left(1-\frac{2W}{3H}\right)^{3/2} \qquad (5)$$

Three levels of ED were selected to validate the model. These values were identified to be representative of the range of ED for which ablation did not involve thermal damage, heat diffusion, recast material and unpredictable groove profiles. The relationships giving the surface roughness as a function of hatch distance are plotted in Fig. 3.9.

Table 3.1 Laser parameters considered to obtain the three levels of ED compared in Fig. 3.7

Set	ED [J/mm²]	P [W]	V [mm/s]
01	1.32	20	433
02	0.66	10	433
03	0.33	10	867

As shown in Fig. 3.9, the higher the energy density (ED), the higher is the predicted surface roughness (S_a). Moreover, surface roughness initially increases with hatch distance up to a certain value depending on the energy density value and then decreases slightly. The stated trend means that, with the assumed hypothesis, a value of hatch distance offering a maximized surface roughness always exists and could be used for further analysis to increase the contact area between the adhesive and the adherend.

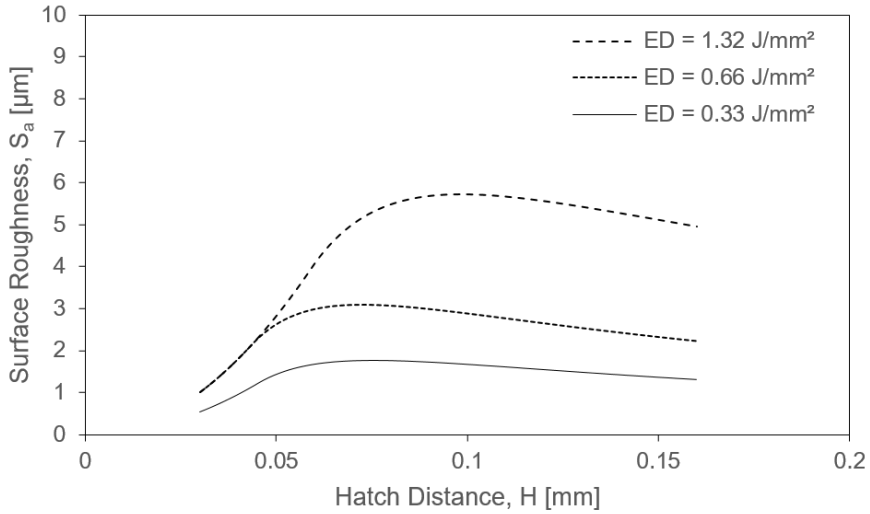

Fig. 3.9: Theoretical behaviors of S_a as a function of H, for surfaces treated with three different ED values.

Morphology maps of treated surfaces are shown in Figs 3.10 (a)-(b). Both of them are obtained for the parameters indicated as “set 02” in Table 3.1. Moreover, this is to mention that morphologies shown in Figs (a) and (b) are produced for hatch distances equal to 0.0375 mm and 0.1125 mm respectively. It can be seen that, for small hatch distances, the overlap between adjacent grooves produces a macroscopically smooth surface. Instead, when the hatch distance is wider than the grooves width, as shown in Fig. 3.10 (b), a portion of the initial surface remain untreated. Moreover, a significant amount of debris can be noticed on the grooves sides.

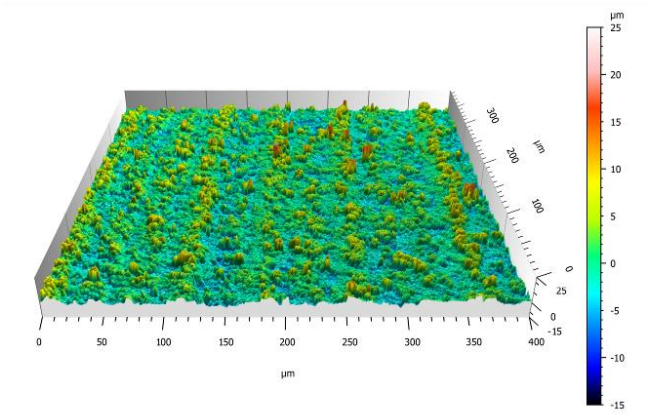

(a)

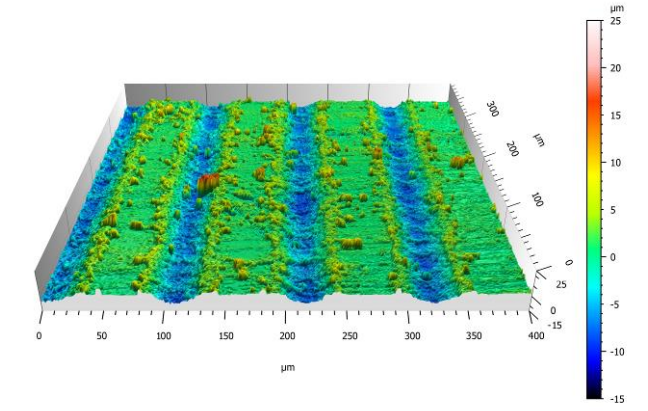

(b)

Fig. 3.10: Morphology maps of surfaces produced with (a) P = *10* W, V = *433 mm/s,* H = *0.0375 mm, (b)* P = *10W,* v = *433 mm/s,* H = *0.1125 mm.*

It should be noted that the simplified model proposed above takes into account a simple ablation mechanism. The proposed model may show drawbacks for high values of energy density which generate a vigorous expulsion of debris and recast material along the edges of the groove. In fact, residuals may hinder the definition of a preliminary surface roughness represented by the direction of the flanked grooves.

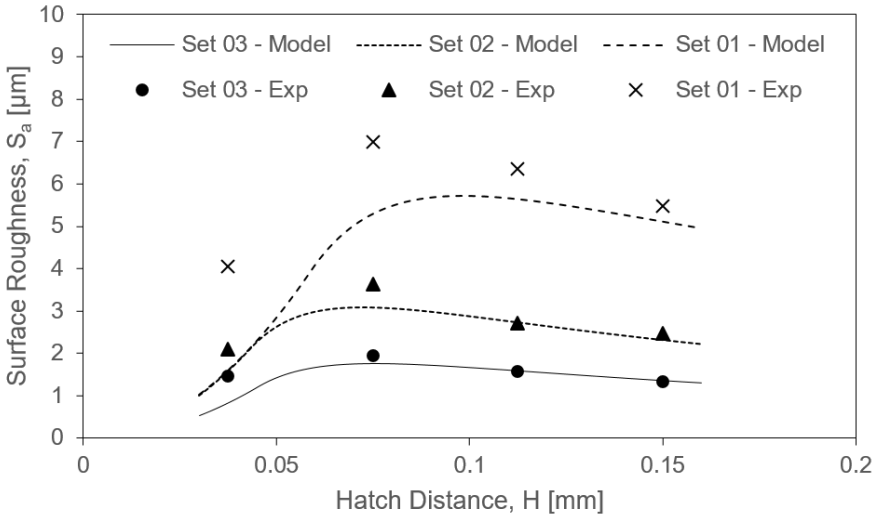

Fig. 3.11: Comparison of measured S_a with the theoretical trends of Fig. 3.7 as a function of H.

This fact is demonstrated in Fig. 3.11, i.e., the greater accuracy in the roughness prediction is obtained for the sets 02 and 03 (refer to Table 3.1) characterized by relatively small values of energy density, and the underestimation of the experimental measures is observed when the prediction is made for set 01 characterized by a higher level of energy density.

Moreover, the model underestimates the roughness also for small hatch distance. Here, theoretically, the profile generated by adjacent parabolic functions would result in a very smooth surface. Again, debris produced by the ablation of other grooves makes the surface rougher concerning the surface generated merely by ablation

From the result shown in section 3.3, it can be concluded that the surface morphology and the consequent average surface roughness of a laser treated surface can be accurately predicted within a specific range of energy density, using analytical relationships, i.e., from the knowledge of the lasing parameters.

3.4 Optimization of laser surface roughness-mediated joining process parameters

From the analytical model developed in the previous section, it is evident that surface roughness is a function of surface groove characteristics (e.g., groove width, W, and groove depth, D) and one of the laser surface treatment parameters (e.g., hatch distance, H). Each of groove characteristics is, again, a function of energy density, ED (A function of two laser treatment parameters like average laser power, P and scanning speed, V for a constant laser spot diameter). Hence, from the analytical model, it can be concluded that the surface characteristics and the consequent average roughness of a laser treated surface can be accurately predicted from energy density and hatch distance, i.e. from the knowledge of laser surface treatment parameters. Besides, surface roughness can be precisely designed, modified and controlled through proper selection and regulation of the aforestated surface treatment parameters.

However, it is hard to achieve a clear relationship between the joint fracture load and the surface roughness and in turn the energy density. Because the wedging effect obtainable at low S_a is overcome by a further phenomenon related to the entrapment of air bubbles. In [20], it was ascertained that the number and the size of air bubbles increase with increasing the roughness thus representing weak points in which a very high notch effect can be reached. Fig. 3.4 shows this behavior at a constant value of the hatch distance and for an energy density value generating a reproducible roughness characterized by well-spaced grooves. Conversely, when hatch distance is relatively small, or the energy density is high, the grooves interact with each other, and they can be partially filled with debris and recast material expulsed from adjacent ones with a more chaotic distribution of peaks and valleys. This fact apparently makes the surface morphology more complex and challenging to be predicted.

A statistical approach is, therefore, employed to analyse the experimental data within a DOE framework to avoid the difficulties in formulating an analytical model linking the entrapment phenomenon of the bubbles, areal roughness, and finally the joint fracture load; and to globally understand the effect of laser surface treatment parameters on the joint fracture load as well. An easy way to estimate a first-degree polynomial model is to use a factorial experiment or a fractional factorial design to ascertain which input variables affect the response variable(s) of interest. But, if it is uncertain that only significant input variables are left, then a more complicated design, such as a central composite design based on response surface methodology (RSM) can be implemented to estimate a second-degree polynomial model, which is still only an approximation at best. However, the second-degree model obtained can be used to optimize (maximize, minimize, or attain a specific target for) the process input variable. That is why, as a try-out, the response surface methodology (RSM) has been used in this study to develop a simple but effective statistical model for joint fracture load alone and to avoid the apparent difficulties in correlating the areal roughness with the joint fracture load. Moreover, to ensure maximum fracture load of the joint, an optimal set of laser surface treatment parameters were determined so that the surface roughness can be designed and controlled at an optimal level using the analytical model developed and presented in section 3.3.

3.4.1 Development of statistical models

At this stage, the fit summary in the design-expert software is used to choose the models that best describe the response factors. The fit summary includes sequential model sum squares to select the highest order polynomial where additional terms are significant, and the model is not aliased. Also, model summary statistics of the fit summary focuses on the model that

maximizes adjusted R-squared and predicted R-squared values. The sequential F-test and lack-of-fit test are carried out using the same statistical software package to check if the regression model is significant and to find out the significant model terms of the developed models as well. The backward elimination regression method is also applied to eliminate the insignificant model terms automatically.

3.4.2 Response model selection

Appropriate response models for the response factors are chosen based on the fit summaries. From the fit summary output of the measured responses shown in Tables 3.2 – 3.3, it is evident that quadratic model is statistically significant for the joint fracture load and hence, it can be used for further analyses.

Table 3.2: Sequential model sum of squares for joint fracture load

Source	Sum of Squares	df	Mean Square	F Value	p-value Prob > F	
Mean	2.335E+8	1	2.335E+8			Suggested
Linear	1.030E+5	3	34329.15	0.17	0.9149	
2FI	2.348E+5	3	78271.43	0.34	0.7966	
Quadratic	1.780E+6	3	5.935E+5	4.91	0.0239	Suggested
Cubic	6.578E+5	4	1.644E+5	1.79	0.2499	Aliased

Table 3.3: Model summary statistics for joint fracture load

Source	Std. Dev.	R^2	Adj. R^2	Pred. R^2	PRESS	
Linear	448.95	0.0309	-0.1508	-0.6212	5.395E+6	
2FI	479.59	0.1015	-0.3132	-1.8303	9.419E+6	
Quadratic	347.80	0.6365	0.3094	-1.0793	6.920E+6	Suggested
Cubic	303.28	0.8342	0.4749	-2.5186	1.171E+7	Aliased

3.4.3 ANOVA analyses

The test for significance of the regression models and the test for significance of individual model coefficients is performed using the same statistical package. During a preliminary analysis, a model to predict 'Joint Fracture Load' was developed by taking into consideration all the input variables (i.e., laser power, scanning speed, and hatch distance). Nevertheless, the model developed did not fit the experimental data and hence, failed to estimate the change in response variable with the change in input variables. Therefore, a revised model was implemented by eliminating the input variables (i.e., laser power, and hatch distance) whose variation did not cause a substantial change in the response variables. This was done by selecting the backward elimination regression method that eliminates the insignificant model terms automatically, the resulting ANOVA Table 3.4 for the chosen model summarizes the analysis of variance of the response and illustrate its significant model terms as well. Besides, individual row of this ANOVA Table demonstrates the following statistical descriptions: *Model*: The model-row shows how much variation in the response is explained by the model along with the over-all model test for significance; *Terms*: The term-row shows how much variation in the response is explained by the associated model term along with its test for significance; and *Residual*: The residual row shows how much variation in the response is still unexplained. Since 'Sum of square' is divided by the degree of freedom to calculate '*Mean square*', in some cases, the value of '*Mean square*' is found to be the same as '*Sum of square*' as the degree freedom associated with that particular 'row source' is unity.

From the table stated above, it is found that calculated Fisher's 'Model-F,' and 'Model-P' values are 9.81 & 0.0015 respectively for joint fracture load model. These 'Model-F' and 'Model-P' values indicate that the selected model is highly significant and there is only a less than 0.01% chance that this large 'Model-F' value could occur due to noise [21-25]. The associated P values of less than 0.05 for the models (i.e., $\alpha = 0.05$, or 95% confidence level) indicate that the model is statistically significant as stated in

Errore. L'origine riferimento non è stata trovata.6]. The lack-of-fit values of the selected model given in Table 3.5 indicate non-significance, as it is desirable. Also, lack-of-fit F-values imply that lack-of-fits are not significant relative to pure error.

The same ANOVA table shows the other adequacy measures, e.g., R-squared, adjusted R-squared, and predicted R-squared values. Since the values estimated are close to one another and deviations among them are less than 0.20, the estimates and predictions are not biased i.e. stated statistical measures are in logical agreement with one another and indicate significant relationships [21-22]. Moreover, adequate precision compares a range of predicted value at the design points to average prediction error. The adequate precision ratio, in this case, is greater than 4 indicating adequate model discrimination [23-24], i.e., predicted values obtained from this model would not be due to the effect of noise (variables that cannot be controlled during experimentation).

Table 3.4: ANOVA for joint fracture load reduced quadratic model

Source	Sum of Squares	df	Mean Square	F Value	p-value Prob > F	
Model	1.783E+6	2	8.915E+5	9.81	0.0015	Sig.
V	22248.46	1	22248.46	0.24	0.6271	
V^2	1.761E+6	1	1.761E+6	19.38	0.0004	
Residual	1.545E+6	17	90869.04			

R^2 = 0.535 Adj. R^2 = 0.481 Pred. R^2 = 0.405 Adq. Precision = 8.974

Table 3.5: Lack-of-fit tests for the selected model

	Sum of Squares	df	Mean Square	F Value	p-value Prob > F	
For joint fracture load reduced quadratic model						
Lack of Fit	1.043E+6	12	86896.08	0.87	0.6151	Not Sig.
Pure Error	5.020E+5	5	1.004E+5			

From Table 3.4 illustrating the ANOVA results for the reduced quadratic model, it is evident that the linear effect of scanning speed (V), and the quadratic effect of scanning speed (V^2) are the significant model terms. The terms related to the scanning speed V, therefore, appear to be more important than those of power and hatch distance. The broader range of variation of V has an impact on this outcome, as compared to the more limited capabilities of the laser machine regarding power control and focusing lens adjustment. The other model terms are then assumed less significant and thus eliminated by a backward elimination process to improve the model adequacy.

The developed statistical models are, therefore, fairly accurate and can be used for prediction within the same design space. The final models as determined by Design Expert software are given below:

Final Statistical Model for joint fracture (JF) load:

$$JF^3 = 2533.38 + 3.56\ V - 2.83 \times 10\text{-}3\ V^2 \qquad (6)$$

where V should be introduced in mm/s and JF results in kN.

Taking into account the dependence reported above, it is worth mentioning that the terms including the influence of the average power and the hatch distance were just neglected because of their extremely low statistical relevance with respect to those of the scan speed. At this purpose, it should be pointed out that the statistical model does not take into account the physics behind the phenomenon. Nevertheless, a possible explanation could be found in the fact that surface activation providing the highest strength does not foresee the use of high average laser power since the generation of deep valleys is affected by the entrapment of air bubbles. As for the hatch distance, a slight surface activation is almost independent on the superposition of the grooves.

3.4.4 Validation of the developed models

Normality of residual data, the pattern of error variance, the presence of outliers, and the extent of residuals in prediction is checked to ensure statistical validation of the developed model. Since multiple regression assumes that the residuals are normally distributed, it is, therefore, necessary to show whether the residuals – the difference between observed and predicted values obtained from the regression model – are normally distributed or not. In this context, the normality of residual data is verified by plotting the normal probability plot (NPP) of residuals. The dataset is normally distributed if the points on the plot fall fairly close to the straight line [22,24]. The normal probability plots of residual values for joint fracture load are illustrated in Fig. 3.10(a). The experimental points are reasonably aligned with predicted or fitted points suggesting the normality of residual data.

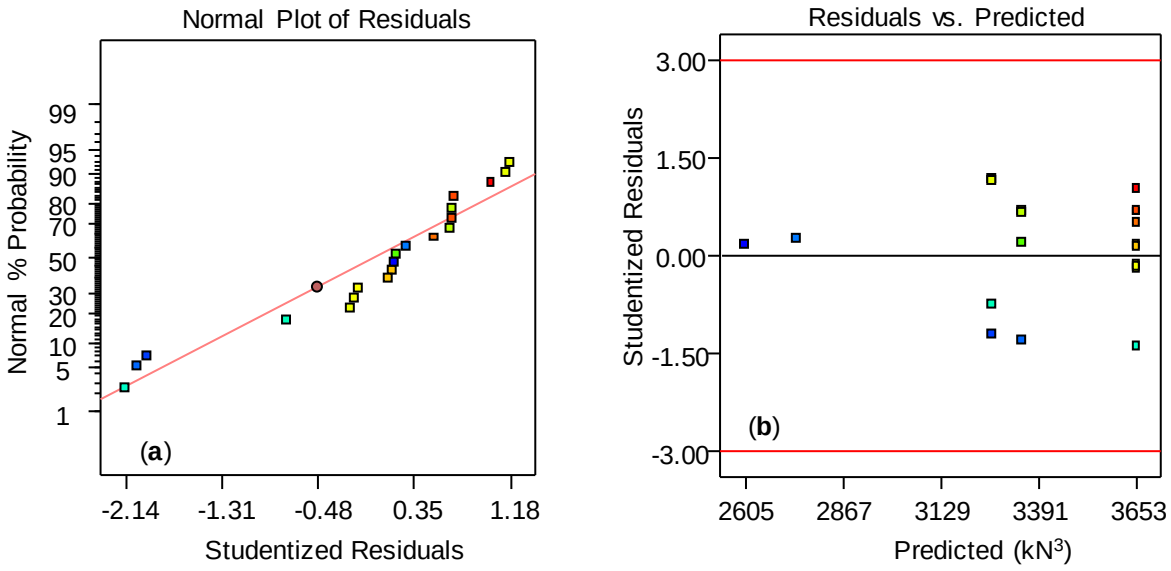

Fig. 3.12: (a) Normal probability and (b) studentized residuals vs predicted plots for joint fracture load

Fig. 3.12(b) illustrates studentized residuals versus fitted values (predicted response) for fracture load of the joint. The residuals are found to be scattered randomly about zero. This randomness of the data indicates the fact that errors have a constant variance for the joint fracture load. Plots of standardized residuals vs. predicted values also show the possible existence of outliers. As shown in the figure, all the points are within ± 2.0σ limits for the response models and confirm no presence of such outliers.

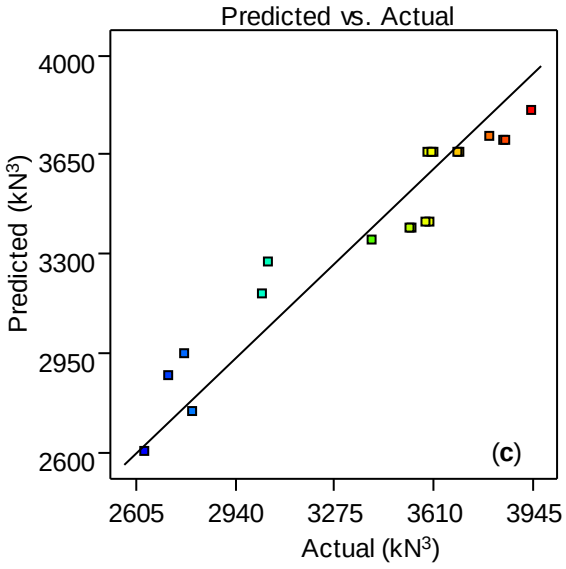

Fig. 3.12 (c): Scatter diagram for joint fracture load

Fig. 3.12(c) is showing the relationship between the actual and predicted values of the joint fracture load. This figure illustrates that the developed model is adequate and predicted results are in good agreement with the measured data as the residuals are close to the diagonal line.

3.4.5 Numerical Optimization

Two criteria have been introduced in this numerical optimization. The first criterion consists in maximizing the joint fracture load with no limitation on laser surface roughness-mediated joining process parameters. In this case, all the process parameters are set within a specified range. Furthermore, the scanning speed is inversely proportional to the time required for the treatment, and the power is an indicator of the energy consumption. Performing the treatment with higher scanning speed and lower average power is therefore of interest in industrial applications, to reduce the treatment costs. Considering the facts mentioned above, the second set of criteria for process parameter optimization are chosen to maximize the joint fracture load and scanning speed and minimize the laser power; whereas hatch distance is kept in the range. Table 3.6 summarizes these two criteria, lower and upper limits as well as the importance of each input and response factor.

Table 3.6: Optimization criteria used in this study

Name	Limit		First Criterion		Second Criterion	
	Lower	Upper	Goal	Importance	Goal	Importance
P (W)	12	18	is in range	3	minimize	5
S (mm/s)	300	1000	is in range	3	maximize	5
HD (µm)	0.05	0.1	is in range	3	is in range	5
JF (kN)	13.813	15.80	maximize	5	maximize	5

Tables 3.7 and 3.8 show the optimal solution based on two optimization criteria as determined by design-expert software. From Table 3.7, demonstrating the optimal bonded joint conditions based on the first set of criteria, it is evident that the largest obtainable joint fracture load is 15.4 kN for the average laser power, scanning speed and hatch distance of 17.73 W, 628.96 mm/s and 0.052 mm respectively. However, with an acceptable adhesive bonded joint fracture load, the laser power can be minimized to its lowest value, i.e., 12 W, the scanning speed can be maximized to 706.28 mm/s and hatch distance ought to be set to 0.055 mm as shown in Table 3.8. Under this condition, the joint fracture load would be 15.39 kN.

Table 3.7: Optimal solutions as obtained based on the first criterion

Solution No.	P (W)	V (mm/s)	H (mm)	Sa (µm)	JF (kN)	Desirability
1	16.72	629.94	0.063	4.306	15.40	0.777
2	15.79	629.25	0.069	4.259	15.40	0.777
3	16.69	629.08	0.085	4.983	15.40	0.777
4	17.60	630.21	0.092	5.617	15.40	0.777
5	16.88	628.97	0.082	5.007	15.40	0.777
6	17.73	628.96	0.052	3.966	15.40	0.777

Again, from Table 3.7 it is clear that, for the first optimization criterion, the optimal ranges of laser power, scanning speed and hatch distance is 12 – 14.5 W, 628.96 – 630.21 mm/s and 0.052 – 0.092 mm respectively. However, as shown in Table 3.8, the optimal range of scanning speed and hatch distance can be increased to 690.9 – 706.2 mm/s and reduced to 0.055 – 0.058 mm respectively if the second set of optimization criteria are applied. As a consequence, any combination of laser surface roughness parameters for the second optimal settings would cause less energy density input for surface treatment. This reduced energy density input, moreover, ensures the preferred surface roughness characteristics and hence leads to greater joint fracture load.

Table 3.8: Optimal solutions as obtained based on the second criterion

Solution No.	P (W)	V (mm/s)	H (mm)	S_a (μm)	JF (kN)	Desirability
1	12.00	690.97	0.055	3.2	15.39	0.845
2	12.00	691.58	0.055	3.2	15.39	0.844
3	12.00	692.79	0.056	3.2	15.39	0.840
4	12.00	706.28	0.055	3.1	15.38	0.837
5	12.00	694.48	0.058	3.2	15.39	0.835

Conclusions

This study aims at designing a surface roughness to enhance the strength of the adhesively bonded joint. In this study, an Nd:YVO_4 laser (λ = 1064 nm) was used for surface modification. Laser power, scanning speed, and hatch distance were used as surface roughness design parameters. Conclusions can be summarized as follows:

- Surface roughness varies nonlinearly with laser-treatment parameters and is energy-limited, i.e., the stated parameters can play a significant role in surface roughness generation and control.
- Surface morphology and the consequent average surface roughness were described by a straightforward model based on the superposition of groove profiles, whose geometry can be linked to the laser parameters. The data calculated by using the model are in good agreement with the experimental measurements up to onset of thermal effects during ablation.
- Conversely from surface roughness, modeling the joint fracture load as a function of process parameters is a complex task from a theoretical point of view. This is because joint fracture load is related to the entrapment of air bubbles on the surface and mechanical interlocking between surface asperities and adhesive. An alternative approach based on Response Surface Methodology was followed to relate the joint fracture load with the meaningful laser parameters.
- Finally, the same statistical approach was used to identify an optimal range of process parameters based on the criterion of joint fracture load maximization. Although the criteria are linked to the specific case of study and the range of variation of the parameters, the authors expect that the optimization proposed could provide general guidelines for similar applications.

Although further study will be required in order to extend the findings of this work to other substrate materials or adhesives (i.e., different adhesive viscosity will affect the air entrapment phenomena), this work provides relevant guidelines in order to maximize the effect of pulsed laser treatment for adhesive bonding.

Acknowledgment

This research was partially supported by the Italian Ministry of University and Research (MIUR), grant SIR RBSI146ZYJ.

References

[1] Yacobi, B.G., Martin, S., Davis, K., Hudson, A., Hubert, M., 2002. Adhesive bonding in microelectronics and photonics. J. Appl. Phys. 91, 6227–6263.

[2] Khan, M.H., Gali, O.A., Edrisy, A., Riahi, A.R., 2016. Effect of oxidation and surface roughness on the shear strength of single-lap-joint adhesively bonded metal specimens by tension loading, Appl. Adhes. Sci. 4, 21-38.

[3] Ghumatkar, A., Budhe, S., Sekhar, R., Banea, M.D., de Barros, S., 2016. Influence of adherend surface roughness on the adhesive bond strength, Lat. Am. J. Solids Struct. 13, 2356-2370.

[4] Uehara, K., Sakurai, M., 2002. Bonding strength of adhesives and surface roughness of joint parts, J. Mater. Process. Technol. 127, 178-181.

[5] de Barros, S., Kenedi, P.P., Ferreira, S.M., Budhe, S., Bernardino, A.J., Souza, L.F.G., 2015. Influence of mechanical surface treatment on fatigue life of bonded joints, J. Adhes. DOI: 10.1080/00218464.2015.1122531.

[6] Rudawska A., Selected aspects of the effect of mechanical treatment on surface roughness and adhesive joint strength of steel sheets. International Journal of Adhesion & Adhesives 50 (2014) 235–243

[7] da Silva L.F.M., Ferreira N.M.A.J., Richter-Trummer V., Marques E.A.S. Effect of grooves on the strength of adhesively bonded joints, International Journal of Adhesion & Adhesives 30 (2010) 735–743

[8] Kim W.S., Yun I.H., Lee J.J., Jung H.T. Evaluation of mechanical interlock effect on adhesion strength of polymer–metal interfaces using micro-patterned surface topography. International Journal of Adhesion & Adhesives 30 (2010) 408 – 417

[9] Alfano, M., Pini, S., Chiodo, G., Barberio, M., Pirondi, A., Furgiuele, F., Groppetti, R., 2014. Surface patterning of metal substrates through low power laser ablation for enhanced adhesive bonding, J. Adhes. 90, 384–400.

[10] Zhang, X.M., Yue, T.M., Man, H.C., 1997. Enhancement of ceramic-to-metal adhesive bonding by excimer laser surface treatment, Mater. Lett. 30, 327-332.

[11] Stammen, E., Dilger, K., Böhm, S., Hose, R., 2007. Surface modification with laser: pre-treatment of aluminum alloys for adhesive bonding, Plasma Process. Polym. 4, 39–43.

[12] Rotella, G., Alfano, M., Schiefer, T. Jansen, I., 2015. Enhancement of static strength and long-term durability of steel/epoxy joints through a fiber laser surface pre-treatment, Int. J. Adhes. Adhes. 63, 87-95.

[13] Buchman A., Rotel M. and Dodiuk-Kenig H. in Mittal K.L., Bahners T., (2015) Laser surface modification and adhesion, Wiley Publishing

[14] Wu Y., Lin J., Carlson B.E., Lu P., Balongh M.P, Irish N.P., Mei Y. Effect of laser ablation surface treatment on performance of adhesive-bonded aluminum alloys. Surface & Coatings Technology 304 (2016) 340–347.

[15] Myers, R.H., Montgomery, D.C., 2002. Response Surface Methodology Process and Product Optimization Using Designed Experiments, second ed. John Wiley & Sons, New York.

[16] Ariaee, S., Tutunchi, A., Kianvash, A., Entezami, A.A., 2014. Modelling and optimization of mechanical behaviour of bonded composite–steel single lap joints by response surface methodology, Int. J. Adhes. Adhes. 54, 30–39.

[17] Heidarzadeh, A., Khodaverdizadeh, H., Mahmoudi, A., Nazari E., 2012. Tensile behaviour of friction stir welded AA 6061-T4 aluminum alloy joints. Mater. Des. 37, 166–173.

[18] Childs, T.H.C., Berzins, M., Ryder, G.R., Tontowi, A.E., 1999. Selective laser sintering of an amorphous polymer: simulations and experiments. Proc. IMechE, Part B: J. Eng. Manuf. 213, 333–349.

[19] ASTM D897-08, 2008. Standard test method for tensile properties of adhesive bonds, American Society for Testing and Materials, West Conshohocken, Pennsylvania (first published in 1949).

[20] Romoli, L., Moroni, F., Khan, M.M.A., 2017. A study on the influence of surface laser texturing on the adhesive strength of bonded joints in aluminum alloys, CIRP Ann. – Manuf. Techn. 66, 237-240.

[21] Kumar, N., Kumar, N., Bandyopadhyay, A., 2018. Optimization of Pulsed Nd:YVO_4 Through Transmission Laser Welding of Transparent Acrylic and Polycarbonate. Materials Today: Proceedings. 5:5235–5243.

[22] Benyounis, K.Y., Olabi, A.G., Hashmi, M.S.J., 2008. Multi-response optimization of CO_2 laser-welding process of austenitic stainless steel. Opt Laser Technol. 40:76–87.

[23] Ruggiero, A, Tricarico, L., Olabi, A.G., Benyounis, K.Y., 2011. Weld-bead profile and costs optimization of the CO_2 dissimilar laser welding process of low carbon steel and austenitic steel AISI316. Opt Laser Technol. 43:82–90.

[24] Acherjee, B., Misra, D., Bose, D., Venkadeshwaran, K., 2009. Prediction of weld strength and seam width for laser transmission welding of thermoplastic using response surface methodology. Opt Laser Technol. 41: 956–967.

[25] Khan, M.M.A., Romoli, L., Dini, G., 2013. Laser beam welding of dissimilar ferritic/martensitic stainless steels in a butt joint configuration. Opt Laser Technol. 49:125–136.

[26] Zulkali, M.M.D., Ahmad, A.L., Norulakmal, N.H., 2006. Oryza sativa L. husk as heavy metal adsorbent: optimization with lead as model solution. Bioresour. Technol. 97, 21–25.